## **CHAPTER 10**

# Irregular Wave Transformation Processes in Surf and Swash Zones

Daniel T. Cox<sup>1</sup>, Nobuhisa Kobayashi<sup>1</sup> and Andojo Wurjanto<sup>2</sup>

ABSTRACT: A frequency-domain model is developed for elucidating the nonlinear transformation processes of the Fourier amplitudes and phases of normally incident random waves in surf and swash zones. The vertically-integrated continuity and momentum equations which have been used to describe a turbulent bore on a beach are rearranged to derive the equations expressing the cross-shore variations of the Fourier components of normally incident random waves. The derived equations are solved numerically using forcing terms computed from a previously developed time-domain model. The frequency-domain model attempts to quantify the importance of the nonlinear forcing due to the cross-shore variations of instantaneous radiation stress and bottom shear stress as well as the seaward boundary condition related to incoming low frequency waves for generating two-dimensional surf beat in the surf and swash zones.

### Introduction

The quantitative understanding of the transformation processes of breaking or broken irregular waves is essential for predicting wave-induced currents and sediment transport in the surf and swash zones. A number of researchers (e.g., Guza andThornton, 1985) have observed that the low-frequency wave components are dominant near the shoreline of gently sloping beaches. The mechanisms by which these oscillations are generated is not fully understood. Guza and Thornton (1985) explained their observations with a standing wave model on the basis of correlations of the incident wave to measured free surface elevations and velocities in the nearshore region. Their analysis was inconclusive, however, regarding the detail mechanisms by which the incident wind waves are modulated to produce the low frequency motions. Symonds et al. (1982) explained the generation of low frequency waves with a time-varying breakpoint model; that is, fluctuations in surf zone width and wave setup lead to the surf beat motions. This model results in a standing wave shoreward of the breakpoint and a progressive wave radiated seaward. More recently, List (1992) proposed a model for two-dimensional surf beat to separate the contributions to the low frequency band by the bound long wave of the wave group envelope and the breakpoint-forced long wave.

In the work presented herein, a frequency-domain model is developed to quantify the importance of the nonlinear forcing due to the cross-shore variations of

<sup>&</sup>lt;sup>1</sup> Center for Applied Coastal Research, Department of Civil Engineering, University of Delaware, Newark, DE 19716

<sup>&</sup>lt;sup>2</sup> Department of Civil Engineering, Bandung Institute of Technology, Jalan, Ganesha 10, Bandung 40132, Indonesia

instantaneous radiation stress and bottom shear stress as well as the seaward boundary condition related to incoming low frequency waves.

First, the time-domain model (TDM) is briefly introduced, including the specification of the incident wave train at the seaward boundary. Next, the computed results are compared with the measured data of Cox et al. (1991) to show that the TDM reasonably predicts the cross-shore variation of the free surface oscillation in the shoaling and surf zones, including the generation of the low-frequency components as well as the shoreline oscillation on a mild slope for irregular waves. The formulation of the frequency-domain model (FDM) is presented in detail, including the model domain, governing equations and boundary conditions. The continuity and momentum equations used in the TDM are rearranged to obtain a linear ordinary differential equation for each Fourier component with nonlinear forcing terms resulting from the interaction of Fourier components. The linear boundary value problem for each harmonic is solved using the nonlinear forcing terms computed by the TDM to avoid solving nonlinear simultaneous equations for Fourier amplitudes The computed cross-shore variations of low-frequency Fourier and phases. amplitudes and phases of the FDM are shown to match those of the TDM. The FDM is then used to examine the effects of each of the nonlinear terms as well as the seaward boundary condition related to incoming low-frequency waves.

# **Time-Domain Model**

A numerical model based on the nonlinear shallow water equations including the effect of bottom friction (Kobayashi *et al.*, 1989) is probably the simplest onedimensional, time-dependent model for predicting the nonlinear time-dependent irregular wave characteristics in the surf and swash zones. Kobayashi and Wurjanto (1992) showed that the TDM could predict available field data on shoreline oscillations fairly well. Moreover, Wise *et al.* (1991) compared the numerical model with the laboratory data of Roelvink and Stive (1989) and obtained reasonable agreement except for undertow and odd velocity moments probably because the model does not account for the vertical velocity variation and is not accurate enough to predict small values of the odd moments.

Cox et al. (1991) conducted a hydraulic model test in a wave flume to obtain detailed data on the cross-shore variations of the free surface oscillations and shoreline oscillation on a 1:20 smooth impermeable slope. Six wave gages were positioned in the shoaling and swash zones at d'=15.0, 12.5, 10.0, 7.5, 5.0 and 3.0 cm, where d' is the depth below the still water level (SWL). Additionally, a runup meter provided the time series of the shoreline oscillations. The target spectrum was based on the Pierson-Moskowitz spectrum, and the waves were generated without regard to nonlinear effects or wave reflection. The data were collected at a sampling interval of 0.04 s with a duration sufficient to include roughly 600 waves.

The seaward boundary of the time-domain model was taken at the location of the most seaward gage at d' = 15.0 cm, immediately outside the breaker zone. The TDM requires that the incident wave time series and not the total time series be specified, where reflection can be significant even for mild slopes, particularly at the lower harmonics. The standard spectral technique of separating incident and reflected waves using an array of gages was not employed since the experiment was originally intended for other purposes (Cox *et al.*, 1991). Instead, the incident wave train to be specified was determined by an iterative technique based on a modification of the measured time series at d' = 15.0 cm as follows. From previous work on this data set, it was estimated that the reflection coefficient was near unity for harmonics less than

half of the peak frequency and near zero for harmonics greater than half of the peak frequency. As a first approximation, the Fourier coefficients of the measured time series were modified as follows:

$$(a_n)_{\text{mod}} = \begin{cases} \frac{1}{\sqrt{2}} a_n; n=1, 2, ..., N_{p/2} \\ a_n; n=N_{p/2}+1, ..., N_{nyq} \end{cases} \text{ and } (b_n)_{\text{mod}} = \begin{cases} \frac{1}{\sqrt{2}} b_n; n=1, 2, ..., N_{p/2} \\ b_n; n=N_{p/2}+1, ..., N_{nyq} \end{cases}$$

where  $a_n$  and  $b_n$  are the real and imaginary parts, respectively,  $N_{p/2}$  indicates the harmonic corresponding to half of the peak frequency, and  $N_{nyq}$  indicates the harmonic corresponding to the Nyquist frequency. The modified time series,  $\eta'_{mod}$ , was recovered by an inverse Fourier transform. To begin the iterative procedure, the modified time series  $\eta'_{mod}$  was specified as the incident wave time series,  $\eta'_1$ . For subsequent iterations, the computed reflected wave time series was subtracted from the assumed (modified) wave time series to obtain the new incident wave time series. After the second iteration, an incident wave time series was obtained that when added to the computed reflected wave time series nearly equaled the total measured time series at d' = 15.0 cm. This incident wave time series after the second iteration is used in the following.

The reference wave height, H', and period, T', for normalization of the TDM computations (Kobayashi and Wurjanto, 1992) were chosen as H' = 6.094 cm and T' = 1.72 s, respectively, based on the spectral estimate of the significant wave height and spectral peak period of the incident wave train,  $\eta_i = \eta_i'/H'$ , at the seaward boundary. The prime denotes a dimensional quantity unless otherwise stated. The duration of the time series specified to the TDM was  $-20 \le t \le 520$ , where t is the time normalized by t=t'/T' and t=-20 is the start of the computation. To eliminate transitional effects in evaluating the TDM and FDM, the initial part of all the time series was truncated for  $-20 \le t \le 520$ . The corresponding band width of the normalized frequency,  $f^*$ , is  $\Delta f^* = .00192$ , where  $f^* = 1$  corresponds to the spectral peak of the incident wave spectrum. The spectra presented herein are smoothed using ensemble averaging to give 40 degrees of freedom and corresponding band width of  $\Delta f_{sm}^* = .0384$ .

The friction factor, f', is the only empirical parameter specified to the TDM. The value f' = 0.01 was used in the computed results presented herein. The model was not sensitive to f' for the range  $0.01 \le f' \le 0.05$  for most of the shoaling and surf zones, although it did have some effect in the swash zone where frictional effects are noticeable (Kobayashi and Wurjanto, 1992).

Figs. 1a to 1f compare the normalized spectral densities,  $S_{\eta}$ , of the measured and computed free surface elevation,  $\eta$ , plotted for the frequency range  $\Delta f_{sm}^* \leq f^* \leq 3.5$  at the six locations in the shoaling and surf zones. The normalized horizontal coordinate, x, is defined as  $x = x'/(T \sqrt{gH'})$ , and the still water shoreline is at x = 2.26. The agreement in Fig. 1a, located at the seaward boundary, indicates the necessity and partial justification of the iterative technique to specify the incident wave train. It is noted that the computed results using the measured time series as the incident wave train showed an overprediction of the lower harmonics by a factor of roughly two in a figure similar to Fig. 1a. Figs. 1b to 1f show that the TDM can be used to predict the free surface oscillations of irregular waves over a mild slope, including the low frequency components. The disagreement in Figs. 1e and 1f in the low frequency components may be partly due to the measurement difficulties at small

water depths. Fig. 2 shows the measured and computed cross-shore variation of setdown or setup,  $\overline{\eta}$ , as well as the node locations where the TDM output was stored. The storage of the TDM output is discussed in further detail in the next section.

Fig. 3 shows the normalized spectral densities,  $S_z$ , of the measured and computed shoreline elevation above SWL for the range  $\Delta f_{sm}^* \leq f^* \leq 3.5$ . The shoreline oscillations are well predicted by the TDM over the entire frequency range of interest, and Fig. 3 shows the dominance of the low-frequency motion. The friction factor f' = 0.01 is used for Fig. 3, and the computed shoreline oscillations for f' = 0.02 and 0.05 were somewhat smaller than that shown in Fig. 3.

### **Frequency-Domain Model**

A frequency-domain model for normally incident irregular waves on a beach of arbitrary geometry but alongshore uniformity is developed herein to examine the nonlinear wave interactions and elucidate the generation mechanisms of low-frequency waves in the surf and swash zones. The FDM is based on the same continuity and momentum equations as the TDM of Kobayashi and Wurjanto (1992). These equations, where the primes indicating the dimensional variables are omitted for brevity, are rearranged as

$$\frac{\partial (\eta - \overline{\eta})}{\partial t} + \frac{\partial q}{\partial x} = 0 \tag{1}$$

$$\frac{\partial q}{\partial t} + g \,\overline{h} \frac{\partial (\eta - \overline{\eta})}{\partial x} + g \,(\eta - \overline{\eta}) \frac{\partial \overline{\eta}}{\partial x} = -g \,\overline{h} \frac{\partial \overline{\eta}}{\partial x} - \frac{\partial S}{\partial x} - \frac{\tau_b}{\rho}$$
(2)

with

$$S = qu + \frac{1}{2}g\left(\eta - \overline{\eta}\right)^2 \tag{3}$$

and

$$\tau_b = \frac{1}{2} \rho f' \left| u \right| u \tag{4}$$

where t = time;  $x = \text{horizontal coordinate taken to be positive in the landward direction; <math>\eta = \text{free surface elevation above the SWL; } q = \text{volume flux per unit width; } g = \text{gravitational acceleration; } h = \text{total water depth given by } h = (\eta+d) \text{ with } d = \text{water depth below the SWL; } u = \text{depth-averaged horizontal velocity defined as } u = q/h;$  $\tau_b = \text{bottom shear stress; } \rho = \text{fluid density; and } f' = \text{empirical bottom friction factor.}$ The overbar in Eqs. 1–3 denotes time averaging. S defined by Eq. 3 may be termed the instantaneous cross-shore radiation stress since  $\overline{S}$  is the usual radiation stress for the adopted momentum equation (Kobayashi *et al.*, 1989). The time-averaged continuity equation obtained from Eq. 1 yields  $\overline{q} = 0$ . The time-averaged momentum equation used to predict the wave setup  $\overline{\eta}$  where  $\overline{\tau_b}$  is normally neglected.  $\overline{\tau_b}$  is retained herein since the computed low-frequency wave motions in the swash zone may be sensitive to the bottom friction. Subtraction of the time-averaged momentum equation from Eq. 2 yields

$$\frac{\partial q}{\partial t} + g \overline{h} \frac{\partial (\eta - \overline{\eta})}{\partial x} + g (\eta - \overline{\eta}) \frac{\partial \overline{\eta}}{\partial x} = -\frac{\partial (S - \overline{S})}{\partial x} - \frac{\tau_b - \overline{\tau_b}}{\rho}$$
(5)

If the water depth  $\overline{h}$  below the mean water level is known, Eqs. 1 and 5 are linear in terms of the oscillatory components  $(\eta - \overline{\eta})$  and q with zero mean except for the nonlinear terms on the right hand side of Eq. 5, which account for the wave-wave interaction effects.

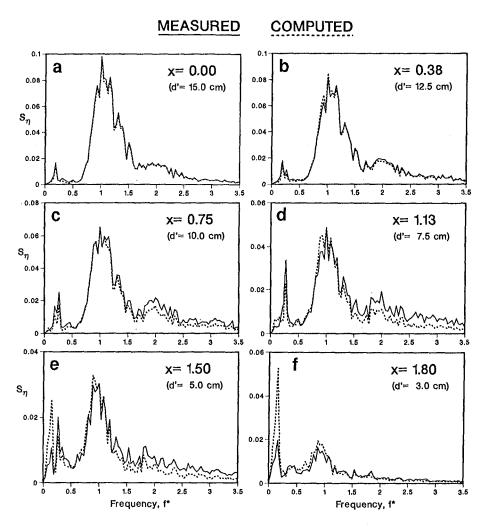
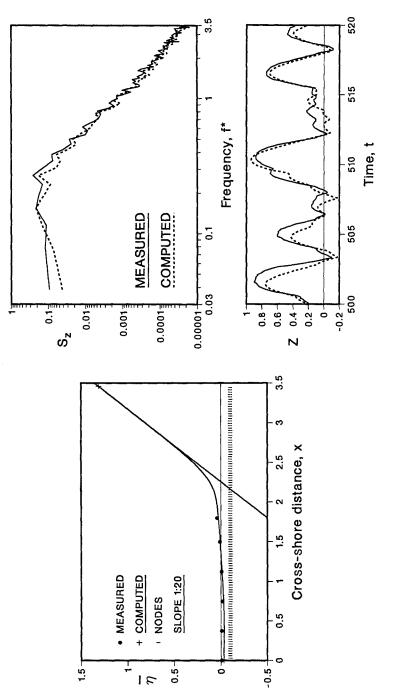


Figure 1: Smoothed spectral densities of normalized free surface elevation,  $\eta$ , as a function of normalized frequency,  $f^*$ , at six locations.



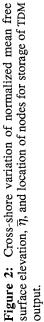


Figure 3: Smoothed spectral density  $S_z$  of normalized shoreline elevation above SWL, Z, as well as corresponding time series.

The time series q,  $\eta$ , S and  $\tau_b$  represented by v(t,x) in the following equation are expressed as Fourier series, *viz.*,

$$v(t,x) = \overline{v} + \sum_{n=1}^{N} \left\{ \operatorname{Re}[v_n(x)] \cos(\omega_n t) + \operatorname{Im}[v_n(x)] \sin(\omega_n t) \right\}$$
(6)

in which  $v_n(x) =$  complex Fourier coefficient with Re and Im indicating the real and imaginary parts of  $v_n$ ;  $\omega_n =$  angular frequency where  $\omega_n = 2\pi n \Delta f^*$ , for n = 1, 2, ..., N and  $\Delta f^*$  is the frequency band width without any smoothing; and N is the number of harmonics. For the FDM proposed herein, Eqs. 1 and 5 are rewritten in terms of the complex Fourier coefficients as follows:

$$-i\,\omega_n\eta_n\,+\frac{dq_n}{dx}=\,0\tag{7}$$

$$-i \omega_n q_n + g \overline{h} \frac{d\eta_n}{dx} + g \eta_n \frac{d\overline{\eta}}{dx} = -\frac{dS_n}{dx} - \frac{\tau_n}{\rho}$$
(8)

Eliminating  $q_n$  from Eqs. 7 and 8 gives

$$g\,\overline{h}\frac{d^2\eta_n}{dx^2} + g\,\frac{d(\overline{h}+\overline{\eta})}{dx}\,\frac{d\eta_n}{dx} + (\omega_n^2 + g\,\frac{d^2\overline{\eta}}{dx^2})\,\eta_n = -\frac{d}{dx}\left(\frac{dS_n}{dx} + \frac{\tau_n}{\rho}\right) \tag{9}$$

The resulting ordinary differential equation for each harmonic is solved using  $\overline{h}(x)$ and the complex Fourier coefficients of  $(S-\overline{S})$  and  $(\tau_b - \overline{\tau_b})$  obtained from q(t,x) and  $h(t,x) = [d(x)+\eta(t,x)]$  computed by the TDM. As a result, the FDM in this paper is not an independent model but supplements the TDM in interpreting the computed results. For the boundary conditions,  $(\eta - \overline{\eta})$  is assumed to be given at the seaward boundary x = 0, while  $(\eta - \overline{\eta})$  is taken to be zero at the location of  $\overline{h} = 0$ . Since  $\overline{h} \ge 0$  in the region wetted by water,  $\overline{h}$  approaches zero asymptotically such that  $\overline{h} = 0$  at the maximum runup location during the specified computation duration. This formulation allows the FDM to be evaluated throughout the swash zone, past the still water shoreline (SWSL) to the point of maximum runup, *i.e.* from x= 2.26 to x = 3.46in the subsequent figures. Further, Eq. 9 can be solved efficiently using a finite difference method of constant grid spacing and a tridiagonal matrix solver (*e.g.*, Press *et al.*, 1989).

The TDM was run twice. First, the model was run to locate the furthest node wetted by water and to determine the locations of the nodes where the output of q(t) and h(t) should be stored with the same sampling rate as the data collection. For the work presented here, there were 461 computational nodes in x with a spatial resolution of  $\Delta x = 0.00752$ . The model was run a second time storing q(t) and h(t) at every four nodes or 116 locations as shown in Fig. 2. Cubic splines were used to interpolate the numerical output from 116 to 461 nodes, and a standard IMSL subroutine was employed to compute the derivatives in Eq. 9.

To evaluate the FDM, a large number of harmonics were chosen from the lowfrequency band. The computed results for  $f^* = 0.198$  and  $f^* = 0.258$  are shown as examples in the following. The frequency  $f^* = 0.198$  represents a harmonic for which x = 0 appears to be an antinode of the cross-shore variation of  $|\eta_n|$ ; and the frequency  $f^* = 0.258$  represents a harmonic for which x = 0 is nearly a node. It is noted that the FDM did not agree with the TDM for frequencies higher than about  $f^* = 0.3$ , probably due to difficulties in computing the cross-shore derivatives of the instantaneous radiation stress at higher frequencies. In the figures to follow, comparisons are made of the magnitude  $|\eta_n|$  and phase,  $\theta_n$ , where Eq.6 for  $\eta(t,x)$  is rewritten

$$\eta(t,x) = \overline{\eta}(x) + \sum_{n=1}^{N} |\eta_n(x)| \cos[\omega_n t + \theta_n(x)]$$
(10)

with

$$|\eta_n| \approx \left\{ \operatorname{Re}[\eta_n(x)]^2 + \operatorname{Im}[\eta_n(x)]^2 \right\}^{\frac{1}{2}}$$
(11)

and

$$\theta_n = \tan^{-1} \left\{ \frac{-\operatorname{Im}[\eta_n(x)]}{\operatorname{Re}[\eta_n(x)]} \right\}$$
(12)

where Eq.12 is computed such that  $-\pi \leq \theta_n \leq \pi$ .

Fig. 4 shows the cross-shore variation of  $|\eta_n|$  and  $\theta_n$  from the TDM and FDM solutions with the measured data for (a)  $f^* = 0.198$  and (b)  $f^* = 0.258$ . The ability of the TDM to simulate the free surface elevations of irregular wave in the surf and swash zones is further exemplified by the agreement between the TDM solutions and measured data. It is emphasized that the TDM and FDM yield continuous solutions landward of the SWSL located at x = 2.26. The agreement between the TDM and FDM solutions shows the ability of the FDM to compute the free surface variation of lower harmonics from the nonlinear forcing of the radiation stress and bottom shear stress terms calculated by the TDM. In Fig. 4a, the seaward boundary, x = 0, appears to correspond to an antinode of the free surface for a standing wave in the nearshore, with a phase shift of  $\pi$  at the nodal location near x = 1.3. Similarly, Fig. 4b shows that the TDM, FDM and measured data are in good agreement. Further, the seaward boundary nearly corresponds to a node of the free surface but the non-zero value of  $|\eta_n|$  and gradual phase shift near x = 1.8 indicates that the low frequency motions are not purely standing in the inner surf zone. The FDM was reformulated to solve for the volume flux,  $q_n$ , instead of the free surface displacement,  $\eta_n$ , from Eqs.7 and 8. The reformulation was also intended to examine the sensitivity of the solutions to the number of differentiations of  $S_n$  and  $\tau_n$  with respect to x. Solutions for the crossshore variation of the magnitude  $|q_n|$  and its phase  $\theta_n$  from the TDM and FDM for  $f^* = 0.258$  are shown in Fig. 5. Figs. 4b and 5 further exemplify the apparent standing wave pattern with nodes of the volume flux corresponding to antinodes of the free surface displacement.

To assess the importance of the nonlinear forcing terms on the right hand side of Eq. 9, the magnitudes of the instantaneous radiation stress and bottom shear stress are examined. Fig. 6 shows the cross-shore variations of  $|S_n|$  and  $|\tau_n|$  for input to FDM for (a)  $f^* = 0.198$  and (b)  $f^* = 0.258$ . The maximum value of instantaneous radiation stress occurs in the breaker zone while the bottom shear stress may become as large as the radiation stress in the swash zone. The oscillations in Fig. 6 are probably caused by the spurious numerical oscillations in the TDM.

A primary purpose of the FDM is to assess the relative importance of the seaward boundary condition and the nonlinear forcing terms. Fig. 7 shows the cross-shore variations of  $|\eta_n|$  and  $\theta_n$  from the FDM for the solutions without and with modifications to the seaward boundary condition and to the nonlinear forcing for (a)  $f^* = 0.198$  and (b)  $f^* = 0.258$ . In Fig. 7a, the FDM solution modified by specifying  $\eta_n = 0$  at x = 0, is greatly affected since x = 0 corresponds to the antinode. Interpretation is somewhat limited, however, because both incident and reflected waves are affected by this boundary condition. It is interesting to note that this solution in the swash zone for  $x \ge 2.5$  is not affected by the boundary condition at x = 0, suggesting the dominance of the nonlinear forcing terms in the swash zone.

163

This result is consistent with all other lower harmonics examined. The FDM solution modified by zeroing both of the nonlinear forcing terms is basically unaffected except in the swash zone. This implies that the wave motion at  $f^* = 0.198$  is essentially a standing wave except in the swash zone. In Fig. 7b, the FDM is modified similarly for  $f^* = 0.258$ . Because x = 0 roughly corresponds to a node of the free surface, the solution is affected only slightly by imposing the condition  $\eta_n = 0$  at x = 0. It is noted that the solution in the swash zone for  $x \ge 2.5$  is unaffected by the seaward boundary condition. By zeroing the nonlinear forcing terms,  $|\eta_n|$  is reduced, but the basic standing wave pattern is apparent with only a slight shifting of the nodal location near x = 1.8. As a whole, Fig. 7 suggests that the wave motion in the swash zone is dominated by the nonlinear forcing rather than the seaward boundary condition and that the relative importance of these two throughout the surf zone depends on the frequency.

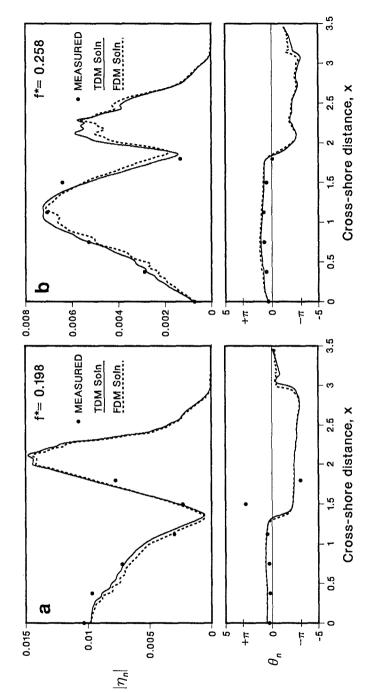
In a further attempt to quantify the relative importance of the radiation stress and bottom shear stress, the FDM is evaluated with modifications to these two terms separately. Fig. 8 shows the cross-shore variations of  $|\eta_n|$  and  $\theta_n$  from the FDM for the three solutions without and with modification to the  $S_n$  and  $\tau_n$  terms. Fig. 8a for  $f^* = 0.198$  shows that the forcing terms do not affect the solution much, consistent with Fig. 7a. Hence, the solutions for  $S_n = 0$  or  $\tau_n = 0$  are similar except that  $S_n$ seems to be the more important of the two in the swash zone. Fig. 8b for  $f^* = 0.258$ shows that the forcing terms individually increase the magnitude  $|\eta_n|$  over most of the surf zone, whereas in Fig. 7b their combined effect is to reduce the magnitude  $|\eta_n|$  by roughly a factor of two. Additionally, Fig.8b shows that  $\tau_n$  affects the magnitude  $|\eta_n|$  but not the phase  $\theta_n$ . For this frequency,  $S_n$  affects the phase  $\theta_n$  somewhat more.

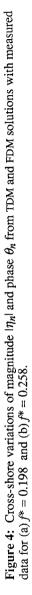
#### Conclusions

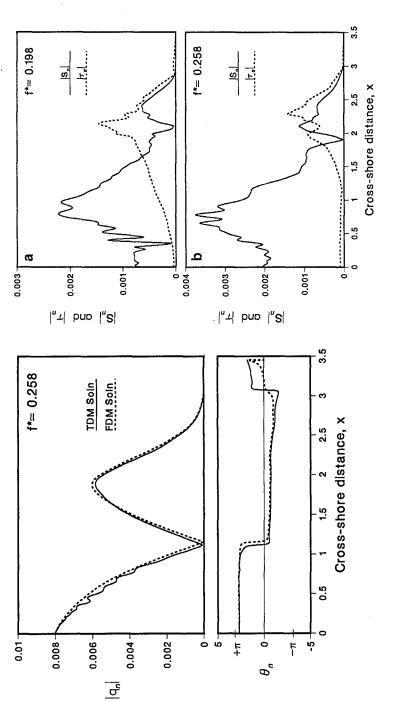
Accurate prediction of the low-frequency motions in the surf and swash zones requires specification of incident low frequency waves immediately outside the breaker zone. At present, no reliable theory is available to predict incident bound long waves immediately outside the surf zone except for the simplified model by List (1992). The TDM was shown herein to predict the temporal and cross-shore variations of the free surface elevation in the surf and swash zones fairly well: however, it does not reveal how and where low-frequency waves are generated or transformed in the surf and swash zones. Additional analyses are hence needed to interpret the computed results. The FDM was proposed to elucidate the nonlinear transformation and generation processes of the low-frequency waves in the surf and swash zones. Important to the formulation of this model was the use of  $\overline{h}$ , eliminating the singularity problem of the free surface elevation in the swash zone. The limited computation for one test run suggests that the low-frequency wave motions in the surf and swash zones appear to be standing waves, qualitatively consistent with the field data and analysis of Guza and Thornton (1985), but modified by the forcing terms associated with the instantaneous radiation stress and bottom shear stress. The degree of modifications depends on specific frequencies.

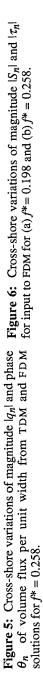
#### Acknowledgment

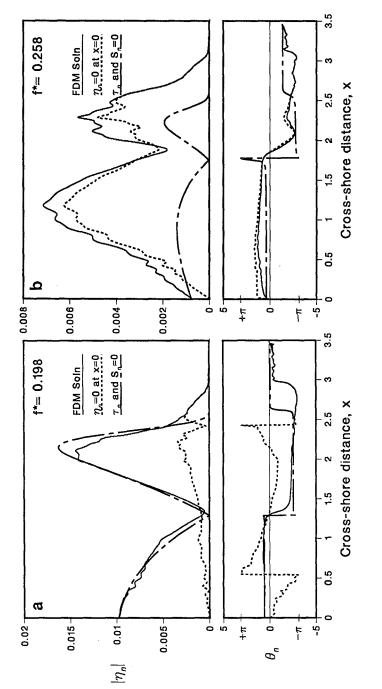
This work is a result of research sponsored by the NOAA Office of Sea Grant, Department of Commerce under grant NA85AA–D–SG033 (SG 92 R/OE–10).



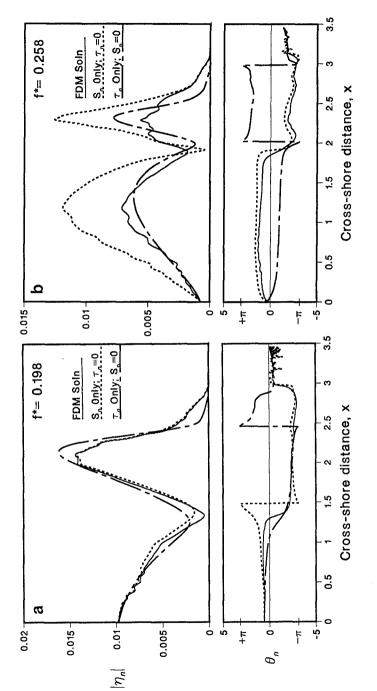














### References

- Cox, D.T., Kobayashi, N. and Mase, H. (1991) "Effects of fluid accelerations on sediment transport in surf zones," *Proc. Coastal Sediments* '91, ASCE, 447-461.
- Guza, R.T. and Thornton, E.B. (1985) "Observations of surf beat," J. Geophys. Res., 90(C2), 3161-3172.
- Kobayashi, N., DeSilva, G.S. and Watson, K.D. (1989) "Wave transformation and swash oscillation on gentle and steep slopes," J. Geophys. Res., 94(C1), 951–966.
- Kobayashi, N. and Wurjanto, A. (1992) "Irregular wave setup and run-up on beaches," J. Wtrway. Port Coast. Oc. Engrg., ASCE, 118(4), 368-386.
- List, J.H. (1992) "A model for the generation of two-dimensional surf beat," J. Geophys. Res., 97(C4), 5623-5635.
- Press, W.H., Flannery, B.P., Teukolsky, S.A. and Vetterling, W.T. (1989) *Numerical Recipes*, Cambridge University Press, Cambridge, U.K.
- Roelvink, J.A. and Stive, M.J.F. (1989) "Bar-generating cross-shore flow mechanisms on a beach," J. Geophys. Res., 94(C4), 4785–4800.
- Symonds, G., Huntley, D.A. and Bowen, A.J. (1982) "Two-dimensional surf beat: Long wave generation by a time-varying breakpoint," J. Geophys. Res., 87(C1), 492-498.
- Wise, R.A., Kobayashi, N. and Wurjanto, A. (1991) "Cross-shore sediment transport under irregular waves in surf zones," *Proc. Coastal Sediments '91*, ASCE, 658– 673.